DOI: 10.13009/EUCASS2025-402
11TH EUROPEAN CONFERENCE FOR AERONAUTICS AND SPACE SCIENCES (EUCASS)

Design and Test of a 1kN LOX/Ethanol Actively Cooled Student Rocket Engine

Paul Marchi†, Mehdi Delouane*, Célian Laurent*, Anica Lekic***
**Innovative Propulsion Laboratory, IPSA*
***IPSA*
Ivry-sur-Seine, France
paul1.marchi@ipsa.fr – mehdi.delouane@ipsa.fr – celian.laurent@ipsa.fr – anica.lekic@ipsa.fr
† Corresponding Author

Abstract
This paper presents the design, development, and testing of a 1 kN LOX/ethanol liquid rocket engine by the Innovative Propulsion Laboratory (IPL) student team at IPSA. Emphasis is placed on regenerative cooling, injector design, and numerical heat transfer prediction. Design choices were guided by analytical and numerical models and validated through hotfire tests. The project yielded valuable technical and hands-on experience in cryogenics, fluid systems, and rocket engine testing. The results demonstrate the feasibility of student-led development of regeneratively cooled engines and lay the groundwork for future flight-capable liquid propulsion systems.

Nomenclature

Symbols				Subscripts	
F	Thrust (N)	v	Velocity (m/s)	e	Exit
$\dot{m}$	Mass flow rate (kg/s)	C_F	Thrust coefficient	g	Gases
P	Pressure (Pa)	γ	Adiabatic constant	t	Throat
c^*	Characteristic Velocity (m/s)	O/F	Oxidizer/Fuel ratio	w	Wall
A	Area (m²)	ζ	Combustion efficiency	ch	Channel
ε	Expansion ratio (A_e/A_t)	λ	Nozzle efficiency	o	Orifice
L^*	Characteristic Length (m)	h	Convection coefficient	c	Chamber
V	Volume (m^3)	c_p	Heat capacity (J/kg K)	opt	Optimal
T	Temperature (K)	ρ	Density (kg/m^3)	amb	Ambient
D	Diameter (m)	μ	Viscosity (Pa s)		
M	Mach number	C_D	Discharge coefficient		
K_{inj}	Injector coefficient	ΔP	Difference in pressure (Pa)		
ΔT	Difference in temperature (K)	Pr	Prandtl number		

1. Introduction

Liquid rocket propulsion remains a complex and multidisciplinary field, traditionally dominated by large institutions and aerospace companies. However, recent years have seen increased interest from academic and student-led teams aiming to develop their own liquid engines as educational and research platforms. This paper presents the work of the Innovative Propulsion Laboratory (IPL), a student team at IPSA, in designing and testing a 1 kN liquid rocket engine using liquid oxygen (LOX) and ethanol. The project aims to develop core competencies in combustion, cryogenics, thermal management, and propulsion system testing. By focusing on an actively cooled design and an in-house developed injector, we seek to validate analytical and numerical models through experimental testing.

2. Design Process

The design process of the rocket engine began in September 2023 and was conducted over the course of six months. The main goal of this engine is to provide hands-on experience in liquid rocketry as well as cryogenic systems to members of the team. To that end, the nominal thrust was chosen to be 1kN, a reasonable goal for a student team with little experience and budget. Hence, ethanol was selected as the fuel due to its ease of handling and low cost. The

DOI: 10.13009/EUCASS2025-402

oxidizer was selected as liquid oxygen (LOX) to give the team experience with cryogens. Last, to simplify test bench design and reduce the heat load, a chamber pressure of 10 bar was chosen as well as a pressure of 0.7 bar at the nozzle exit.

2.1 General sizing

The initial design step entailed selecting the mixture ratio (O/F). Following a bibliographic study and an analysis of the effect of O/F variation on the theoretical I_{sp} as well as the combustion temperature, a mixture ratio of 1.5 was chosen. Values for the combustion temperature $T_{g,c}$, the specific heat ratio γ and the average molar mass of combustion products M were obtained from CEA or RPA software. The combustion efficiency ζ_{c^*} was assumed to be 87% and the nozzle efficiency λ was taken as 98%. These choices lead to the characteristics presented in Table 1 and Table 2 which were calculated using equations 1 to 6.

$$c^*_{theo} = \frac{\sqrt{\gamma r T_{g,c}}}{\gamma\sqrt{\left(\frac{2}{\gamma+1}\right)^{\frac{\gamma+1}{\gamma-1}}}} \quad (1)$$

$$C_{F,theo} = \sqrt{\frac{2\gamma^2}{\gamma-1}\left(\frac{2}{\gamma+1}\right)^{\frac{\gamma+1}{\gamma-1}}\left[1-\left(\frac{P_e}{P_c}\right)^{\frac{\gamma-1}{\gamma}}\right]} + \frac{P_e - P_{amb}}{P_c}\frac{A_e}{A_t} \quad (2)$$

$$c^*_{real} = c^*_{theo}\zeta_{c^*} \quad (3)$$

$$C_{F,real} = C_{F,theo}\lambda \quad (4)$$

$$v_e = c^* C_F \quad (5)$$

$$\dot{m}_{tot} = \frac{F}{v_{e,real}} = \frac{F}{c^*_{real} C_{F,real}} \quad (6)$$

Table 1: Arrax engine characteristics

F_{opt}	1000	[N]	$T_{g,c}$	3123	[K]
P_c	10	[bar]	M	22.04	[g/mol]
P_e	0.7	[bar]	γ	1.13	[-]
O/F	1.5	[-]	$\dot{m}_{LOX}$	0.3	[kg/s]
$\dot{m}_{tot}$	0.5	[kg/s]	$\dot{m}_{eth}$	0.2	[kg/s]

Table 2: Performance parameters

Ideal performance ($\zeta_{c^*} = 1.0$ and $\lambda = 1.0$)			Expected performance ($\zeta_{c^*} = 0.87$ and $\lambda = 0.98$)		
c^*	1710	[m/s]	c^*	1368	[m/s]
$C_{F,opt}$	1.36	[-]	$C_{F,opt}$	1.33	[-]
$v_{e,opt}$	2323	[m/s]	$v_{e,opt}$	1822	[m/s]
$C_{F,atm}$	1.26	[-]	$C_{F,atm}$	1.24	[-]
$v_{e,atm}$	2163	[m/s]	$v_{e,atm}$	1696	[m/s]

To determine the geometry of the engine (see Figure 1), the chamber diameter is set to 90mm, the nozzle will be a cone with a 15° half-angle for ease of machining for the Battleship engine, and an 80% relative length bell nozzle for

DOI: 10.13009/EUCASS2025-402

the cooled engine (i.e. the Arrax engine). The characteristic length L^* of the chamber is chosen to be 1.3m, leading to a relatively high residence time, which should help improve combustion efficiency. The half-angle of the converging section is 25°, which is relatively low, in retrospect, a higher value such as 35 or 40° could have been chosen with little to no impact on performance [3]. All other dimensions can be derived from these dimensions using equations 7, 8 and 9.

$$A_t = \frac{F}{P_c C_F} \tag{7}$$

$$A_c = \varepsilon_c A_t \tag{8}$$

$$V_c = L^* A_t \tag{9}$$

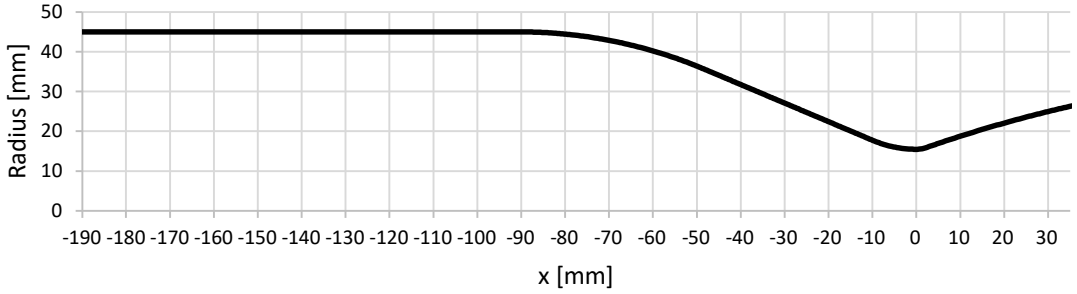

Figure 1: Contour of the Arrax engine (cooled version)

2.2 Uncooled "Battleship" chamber

The Battleship engine serves as a test article for the ignition process. Given the lack of experience of the team in rocket engine design and testing, it was deemed preferable to test ignition on an engine capable of withstanding "hard-starts" and pressure peaks inside the chamber before hotfire testing our more fragile additively manufactured CuCrZr engine.

This engine being uncooled, it relies on conductive heat transfer inside the wall material to dissipate the heat away from the hot wall, meaning that a material with a high thermal conductivity and a high melting point is preferable. Additionally, as mentioned previously, this engine shall have a strong mechanical resistance to internal pressure, making materials with a high tensile strength favorable. Figure 2 presents the yield strength of a few candidate materials as a function of temperature whereas Table 3 shows the room temperature conductivity of these materials.

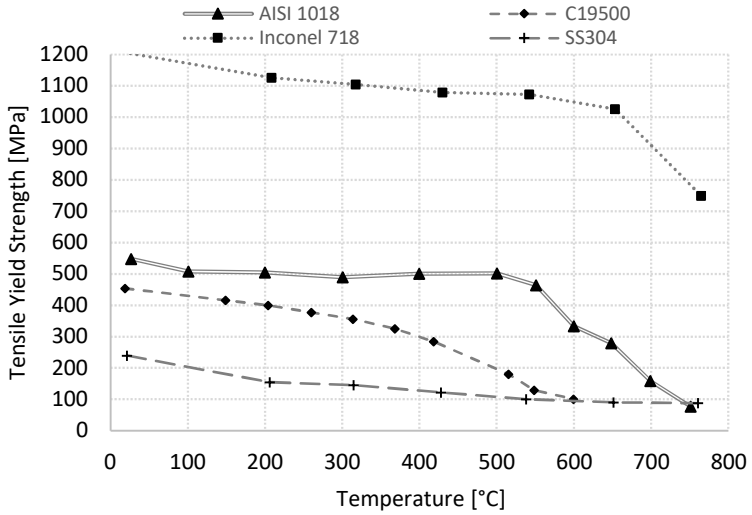

Figure 2: Yield strength of candidate materials vs temperature

DOI: 10.13009/EUCASS2025-402

Table 3: Thermal conductivity of candidate materials

AISI 1018 Steel	51.9 W/(m K)
C19500 Copper	199 W/(m K)
Inconel 718	11.4 W/(m K)
Stainless Steel 304	16.2 W/(m K)

The third element to take into consideration to select the best material for this engine is cost (including both cost of the raw material and cost of machining) since we want the manufacture of the engine to be as cheap as possible. We summarize the three selection criteria in Table 4 to arrive at our material of choice: AISI 1018 carbon steel.

Table 4: Chamber materials overview

	Mechanical strength	Thermal conductivity	Cost
AISI 1018 Steel	++	+	++
C19500 Copper	+	+++	-
Inconel 718	+++	-	--
Stainless Steel 304	-	-	-

To better handle the increased heat flux at the throat, the choice was made to make a throat insert out of brass, which is easy to machine, cheap, and has good thermal conductivity (~117 W/(m K)).

In order to predict the convective heat flux from the hot gases to the chamber wall, the Bartz correlation (eqs. 10 and 11) is used to compute the convective heat-transfer coefficient h_g.

$$h_g = \frac{0.026}{D_t^{0.2}} \frac{\mu^{0.2} C_p}{Pr^{0.6}} \left(\frac{P_c}{c^*}\right)^{0.8} \left(\frac{A}{A_t}\right)^{0.8} \left(\frac{D_t}{R_{curv,throa}}\right)^{0.1} \sigma \tag{10}$$

$$\sigma = \frac{1}{\left[\frac{1}{2}\frac{T_{w,g}}{T_{g,c}}\left(1 + \frac{\gamma - 1}{2} M^2\right) + \frac{1}{2}\right]^{0.68} \left[1 + \frac{\gamma - 1}{2} M^2\right]^{0.12}} \tag{11}$$

The temperature inside the engine at any given time was calculated using a transient heat-transfer simulation with the ANSYS Mechanical software (fig. 3). The final CAD of the engine, displaying the brass insert inside the steel chamber, is shown in fig. 4.

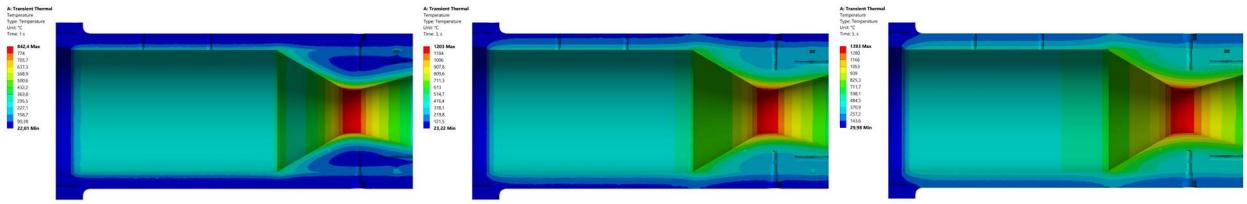

Figure 3: Temperature inside the engine after 1s (left), 3s (middle), and 5s (right)

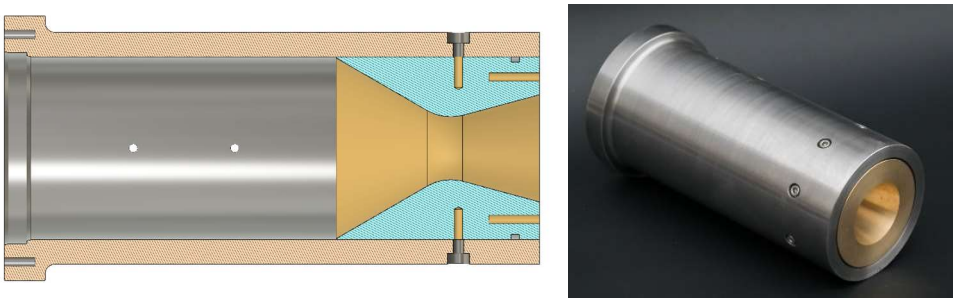

Figure 4: Battleship engine CAD cross-section (left) and after manufacturing (right)

DOI: 10.13009/EUCASS2025-402

2.3 Cooled AM chamber

Since the Innovative Propulsion Lab student team lacked previous experience in predicting heat loads inside a liquid rocket engine, the choice was made to cool our engine with water instead of one of the propellants (typically the fuel), which serves two main purposes:

- Ensure that the engine is sufficiently cooled and avoid the risk of overheating/melting by flowing a high flowrate of water through the cooling channels.
- By measuring the temperature increase of the cooling water, a comparison can be made between the predicted and actual heat flux in the engine, providing valuable data for future engine designs.

The preliminary design of the cooling channels was done with an in-house program using a 1D model for the heat transfer along the wall as well as a 2D conductive heat-transfer calculation to predict the temperature at each point inside the engine wall, especially in the hotter region between cooling channels. The program takes as input the flow properties inside the chamber, the geometry of the engine as well as the data in Table 5 below. The channel dimensions were obtained after using this software several times by iterating the channel dimensions to obtain the desired wall temperatures as well as predict the water exit temperature.

Table 5: 1D heat transfer prediction program inputs

Wall material	CuCrZr		$W_{ch,inj}$	3.0	[mm]
$\dot{m}_{water}$	2	[kg/s]	$W_{ch,conv}$	3.0	[mm]
n_c	50	[-]	$W_{ch,t}$	1.2	[mm]
ε_{wall}	5	[µm]	$W_{ch,e}$	1.4	[mm]
λ_{wall}	355	[W/(m K)]	$H_{ch,inj}$	3.0	[mm]
$T_{l,init}$	15	[°C]	$H_{ch,conv}$	3.0	[mm]
$P_{l,init}$	8	[bar]	$H_{ch,t}$	3.0	[mm]
t_w	1	[mm]	$H_{ch,e}$	3.0	[mm]

To validate the analytical results, a full 3D CFD simulation of the heat transfer in the cooling channels and the pressure drop in the inlet and outlet manifolds was conducted using ANSYS Fluent. The temperature data in the solid domain obtained from this CFD simulation was then used as input data for a mechanical simulation, ensuring that the combined effect of internal chamber pressure and thermal stress across the hot wall did not overcome the material limits.

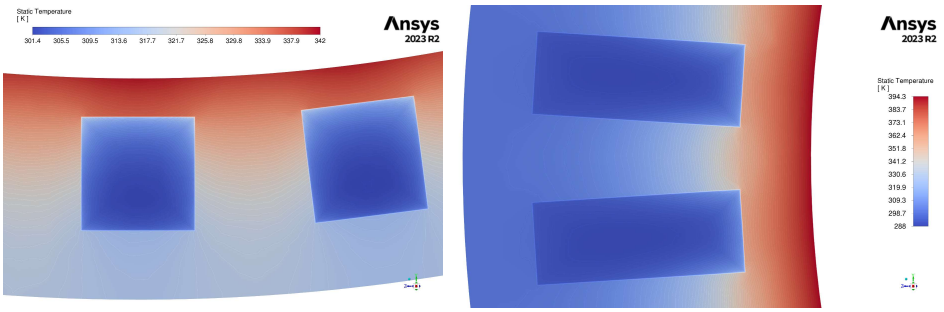

Figure 5: Temperature distribution around the cooling channels in the chamber (left) and at the throat (right)

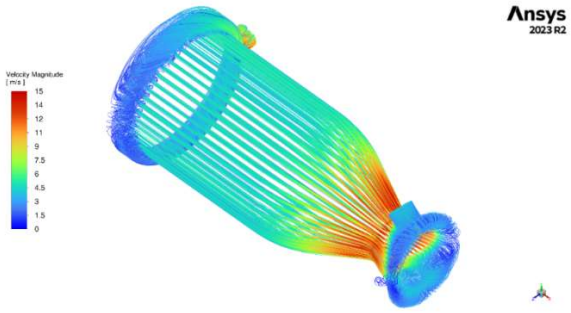

Figure 6: Velocity pathlines of the flow in the cooling channels, displaying the high velocity at the throat and the flow at the manifolds

DOI: 10.13009/EUCASS2025-402

The Arrax engine was additively manufactured (Direct Metal Laser Sintering, DMLS) out of the CuCrZr alloy, which is commonly used in aerospace applications requiring good mechanical strength and excellent thermal conductivity. The part was then heat treated following the Direct Aging Hardening process: The alloy is heated to 490°C in argon for 1 hour and is then cooled to 400°C with argon flow and then let to cool in air. This heat treatment greatly improves the mechanical properties of the alloy, increasing the yield strength to at least 300MPa and the ultimate tensile strength above 420MPa. After heat treatment, the locations requiring lower surface roughness or tighter tolerances were machined and finally the relevant holes were tapped. The engine was designed to avoid overhangs higher than 40°, to make the entire part printable with the nozzle down without supports.

Figure 7: Arrax engine after manufacturing

2.4 Pintle injector

The injection system was designed to be identical for both the Battleship and Arrax (actively cooled) engine. It is made up of two main parts: the fixed pintle injector and the injector plate. Liquid oxygen is ejected from the center pintle radially outwards, and the ethanol is injected as a thin annular film axially towards the throat and impacts the LOX exiting the pintle. The injector holes are sized in order to ensure that the pressure drop across the injection orifices is always at least 20% of the chamber pressure down to 80% of the nominal mass flow rate (i.e. the pressure in the injection manifolds is at least 1.2 times the chamber pressure) to avoid low-frequency combustion instability (chugging) due to coupling between the injected flow and the chamber pressure. The dimensions of the injector calculated from eqs. 12-17 are presented in table 6 below. The injector orifices/slots were assumed to have a discharge coefficient $C_D = 0.6$ for preliminary design. The actual value was then experimentally measured on the finished parts using cold flow tests (0.59 for the annular ethanol injection, 0.61 for the pintle injector).

$$\frac{F_{min}}{F_{nom}} = \frac{\dot{m}_{tot,min}}{\dot{m}_{tot,nom}} = \frac{P_{c,min}}{P_{c,nom}} = 0.8 \quad (12)$$

$$\Delta P_{min} = 0.2 P_{c,min} \quad (13)$$

$$\Delta P_{nom} = \frac{\Delta P_{min}}{\left(\frac{P_{c,min}}{P_{c,nom}}\right)^2} \quad (14)$$

$$A_{tot} = \frac{\dot{m}_{tot,nom}}{C_D \sqrt{2 \rho \Delta P_{nom}}} \quad (15)$$

The orifices diameter on the pintle is calculated knowing the number of orifices using equation 16.

$$D_o = 2 \sqrt{\frac{A_{tot}}{n_o \pi}} \quad (16)$$

DOI: 10.13009/EUCASS2025-402

For the annular injection orifice, the diameter of the outer circle of the annulus is calculated knowing the pintle diameter (i.e. the inner circle of the annulus) using equation 17.

$$D_{annulus} = \sqrt{\frac{4A_{tot}}{\pi} + D_{pintle}^2} \tag{17}$$

Table 6: Injector dimensions

LOX			Ethanol		
D_o	1.0	[mm]	$D_{annulus}$	15.60	[mm]
n_o	28		D_{pintle}	15.00	[mm]

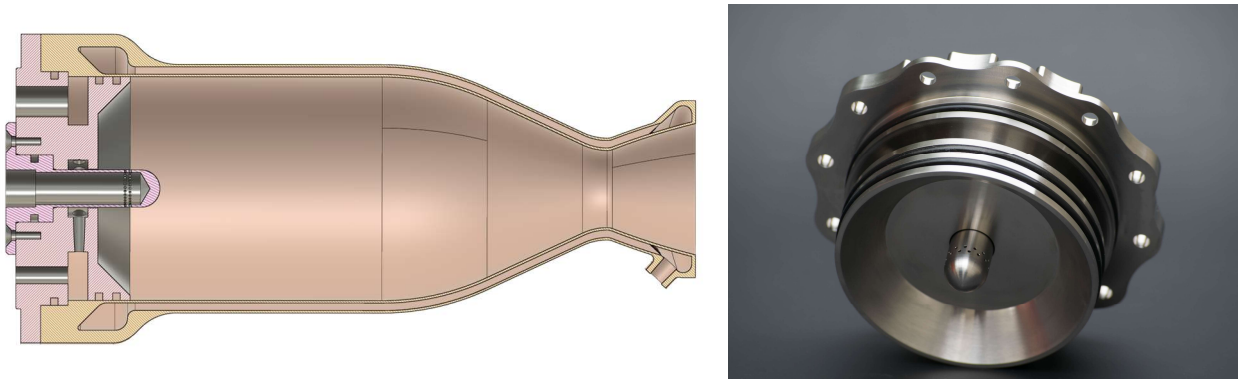

Figure 8: Cross-section of the CAD assembly with the injection system (left) and assembled injector plate (right)

2.5 Ignition system

The ignition system was chosen to be a black powder Klima C2-P solid motor, as they are reliable, relatively safe, and simple of use. The main advantage of the C2 version is the relatively long burn time of around 5 seconds, making timing ignition less constraining. The ignition is triggered by applying voltage across the leads of an electric match inside the motor. Supports were designed to hold the igniter inside the nozzle and break when the chamber pressure rises. This principle is applied to both the Battleship and the Arrax engine, even though the exact models differ, due to difference in nozzle shape between the two versions. Both parts were 3D printed with PLA for ease of manufacturing and time constraints.

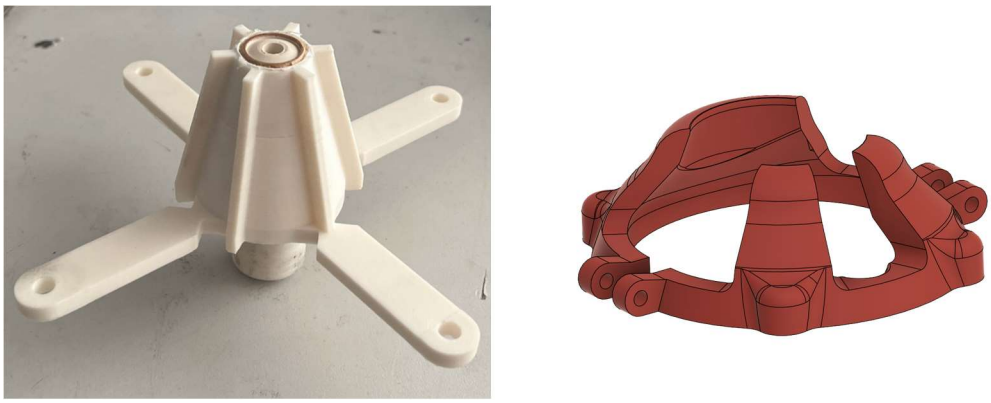

Figure 9: Igniter support with the black powder igniter inside (left) and Arrax engine interface (right)

DOI: 10.13009/EUCASS2025-402

3. Tests

3.1 Test bench setup

After making a Piping & Instrumentation Diagram (P&ID) of our test bench, it was designed in CAD to order the parts needed and assembled after over the course of two months. The structure is made of 40x40mm aluminum T-slot extrusion as well as HPL panels. For the fluidic lines, 10mm and 15mm OD seamless tubes were mainly used.

The ethanol goes through two solenoid valves during nominal operation: SV22 and SV23, where SV23 is an independent redundancy operated separately via a button, allowing us to abort at any time even in case of complete communication loss. During the engine startup, the fuel initially goes through SV24, bypassing the two main valves to have a lower mass flow rate, ensuring a smoother startup than if the full flow was to be ignited. The LOX line follows a similar process. In the case of LOX, since it is cryogenic and it is necessary to ensure that it is liquid in the injector, temperature sensors are placed before the injection to measure the temperature of the line for the chilldowns. Additionally, the LOX line also features relief valves in every location where LOX can potentially be trapped. The fuel and LOX tanks are pressurized by a main nitrogen tank at 50bar. Bang-bang pressurization is used with two solenoid valves in order to maintain the correct pressure inside the two propellant tanks (see Figure 10).

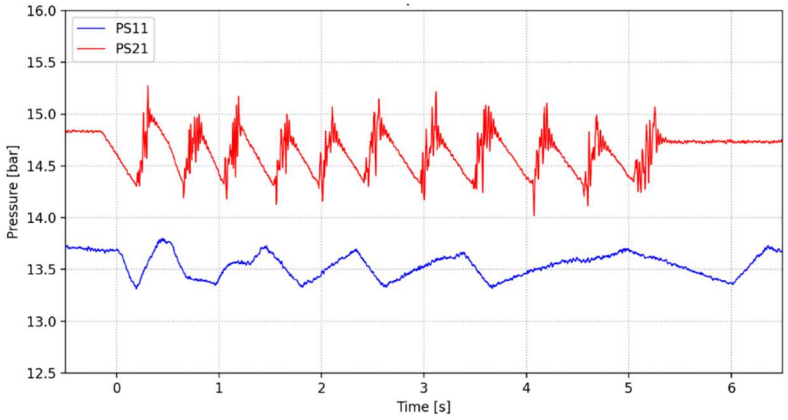

Figure 10: Pressure inside the ethanol (red) and LOX (blue) tanks during a hotfire test, showcasing bang-bang regulation around the setpoint (14.7 bar for ethanol and 13.5 bar for LOX)

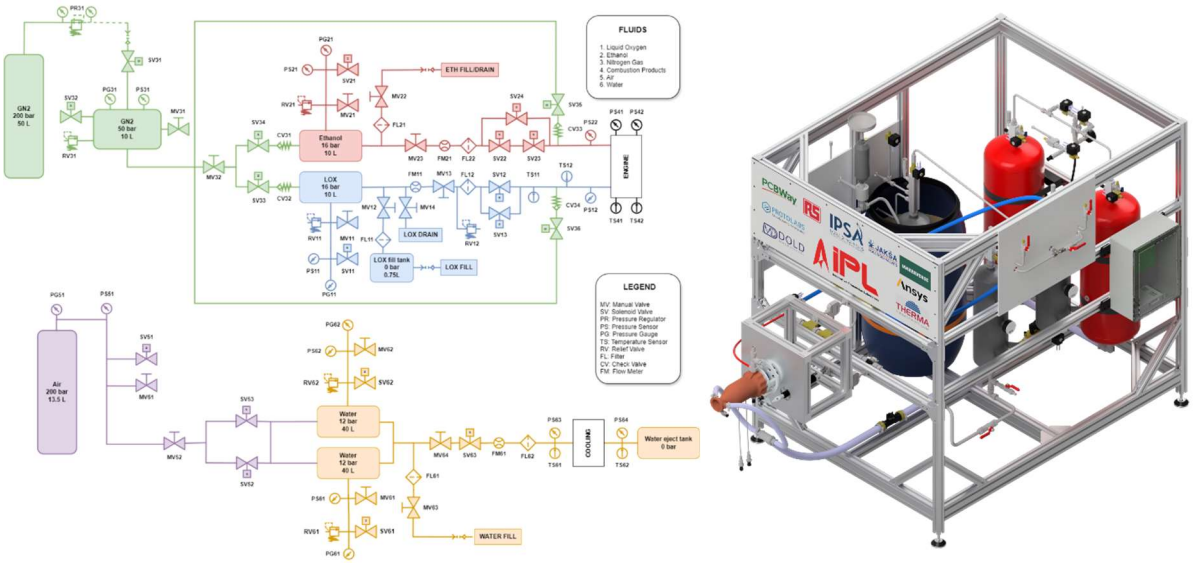

Figure 11: P&ID of the custom test bench (left) and CAD render of the test bench (right)

DOI: 10.13009/EUCASS2025-402

3.2 Data acquisition and logging system

In order to interface with the sensors and solenoid valves on the test bench, a custom PCB was designed, featuring 13 0-5V sensor inputs, 3 4-20mA inputs, 6 thermocouple conversion circuits, 19 24VDC outputs for solenoid valves, a 24V output excitation voltage for the load cells, a 12VDC output for the igniter as well as a dual digital potentiometer. The test bench is controlled by a Teensy 4.1, chosen for its high clock speed, broad I/O, ease of use and low cost. The data from the sensors is acquired at 500Hz by the Teensy and then logged on an SD card and transmitted over Ethernet to the control station computer downrange.

Every hotfire test sequence is defined by a list of parameters, including timings and delays, target pressures, temperature threshold, maximum chilldown number and checked sensor values. These parameters then define a test, which is executed using a state machine by the Teensy in the test bench. Before, during and after every hotfire, the Teensy also continuously checks the values of all the sensors and sends warnings or critical warnings to the control station in case of issue. It is programmed to avoid dangerous situations, such as venting a tank if its internal pressure goes above a certain threshold.

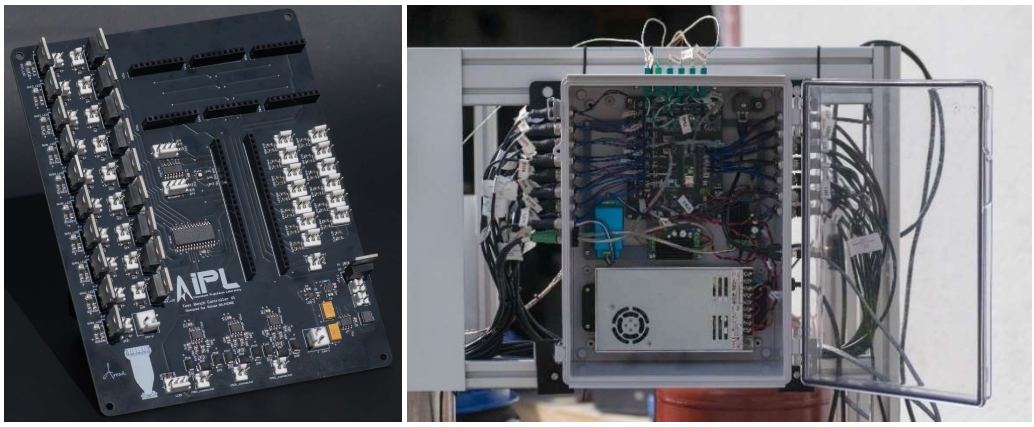

Figure 12: Custom PCB (left) and electronics case installed on the test bench (right)

3.3 Test bench user interface

A custom Human-Machine Interface (HMI) was developed in Qt using C++ to provide real-time monitoring and control of the test bench. The interface is organized into four main tabs, each targeting a specific subsystem:

The *Engine cycle* and *Cooling cycle* tabs allow the operator to directly control the valves and monitor sensor data associated with the propulsion and cooling subsystems, respectively. Both tabs feature interactive Piping and Instrumentation Diagrams (P&IDs), where live sensor values (pressures, temperatures, flow rates) are updated in real time and valve states can be commanded through the graphical interface, enabling fast and easy control of the fluidic systems.

The *Test tab* is structured into distinct sections that allow for flexible test configuration and supervision. It includes a dedicated interface for testing the bang-bang control logic independently, as well as a separate actuator control section for manually operating valves and components without running a full sequence. A third section enables the selection, configuration, and initiation of complete test sequences, which are transmitted to the microcontroller for execution. An integrated emergency stop function and a live event log provide safety and traceability throughout the process. Finally, the *Graph* tab offers flexible plotting capabilities for all sensor values, allowing the user to select and visualize sensor data history in real time or post-test review.

Communication with the Teensy 4.1 microcontroller is handled bidirectionally via UDP, with multithreaded management of data acquisition, parsing, command transmission, and interface updates. The system operates at a default frequency of 20 Hz during setup and pre-test operations—sufficient for valve checks and general system validation—and automatically switches to 500 Hz during hotfire sequences to enable high-resolution data capture and responsive control. All sensor data and control parameters are logged in real time to CSV files, while system events and operator interactions are recorded in parallel as human-readable text logs for traceability.

DOI: 10.13009/EUCASS2025-402

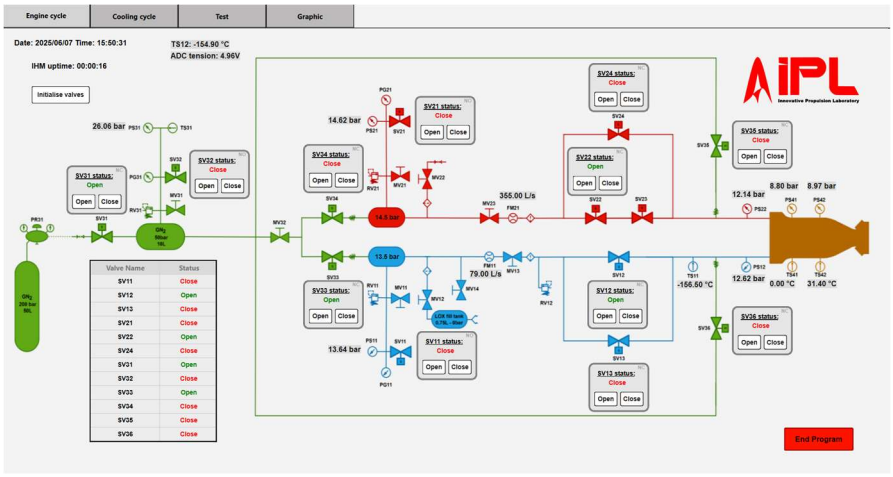

Figure 13: *Engine cycle* tab

4. Results

4.1 Cold flow and cryogenic tests

Cold flow tests were done to characterize the thrust chamber's parameters, such as the coefficient $C_d A(2\rho)^{0.5}$ of the injector, which is essential to estimate the mass flow rate of propellant going through the injection. The coefficient $C_d A(2\rho)^{0.5}$ is a constant for each of the injectors (assuming the density of the injected propellants does not vary during the test) which we denote K_{inj}. As such, when the K_{inj} of the injector is obtained, we can estimate the pressure difference ΔP needed across the injector to obtain the desired mass flow rate, as well as estimate the mass flow rate from pressure data during post-processing.

$$\dot{m} = C_d A\sqrt{2\rho\Delta P} \tag{18}$$

$$\dot{m} = K_{inj}\sqrt{\Delta P} \tag{19}$$

After various tests, we obtain the following results for the LOX injector:

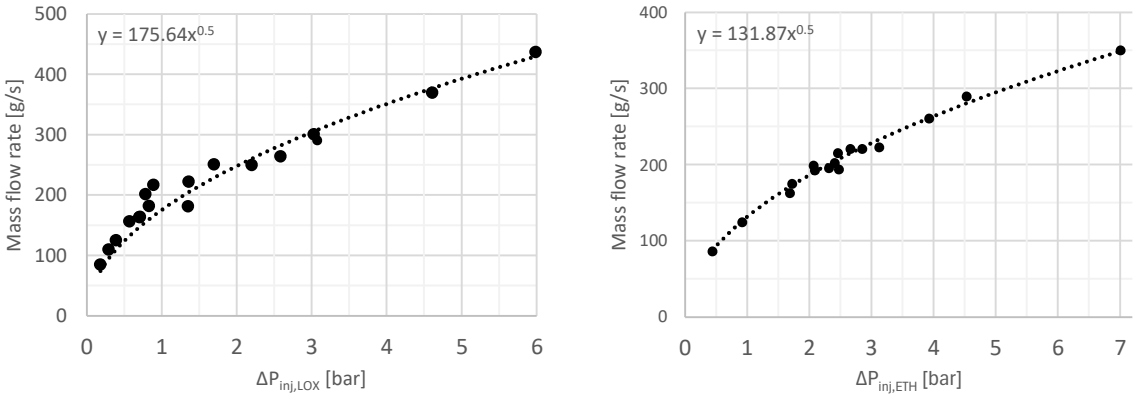

Figure 14: Water mass flow rate through the LOX (left) and ethanol (right) injectors as a function of injection pressure

The data points were fit with a square root law with a coefficient $K_{LOX_{water}} = 175.64\ \mathrm{kg}^{0.5}\mathrm{m}^{0.5}$ and $K_{ETH_{water}} = 131.87\ \mathrm{kg}^{0.5}\mathrm{m}^{0.5}$.

Table 7: Water, LOX and ethanol densities used

ρ_{water}	1000	[kg/m^3]
ρ_{LOX}	1200	[kg/m^3]
ρ_{ETH}	790	[kg/m^3]

DOI: 10.13009/EUCASS2025-402

The difference in density between the water and the propellants was accounted for using the data in Table 7. From eq. 20, the adjusted coefficients are therefore $K_{inj_{ETH}} = 118\ \mathrm{kg}^{0.5}\mathrm{m}^{0.5}$ and $K_{inj_{LOX}} = 192\ \mathrm{kg}^{0.5}\mathrm{m}^{0.5}$.

$$K_{adj} = K_{inj}\sqrt{\frac{\rho_{fluid}}{\rho_{water}}} \tag{20}$$

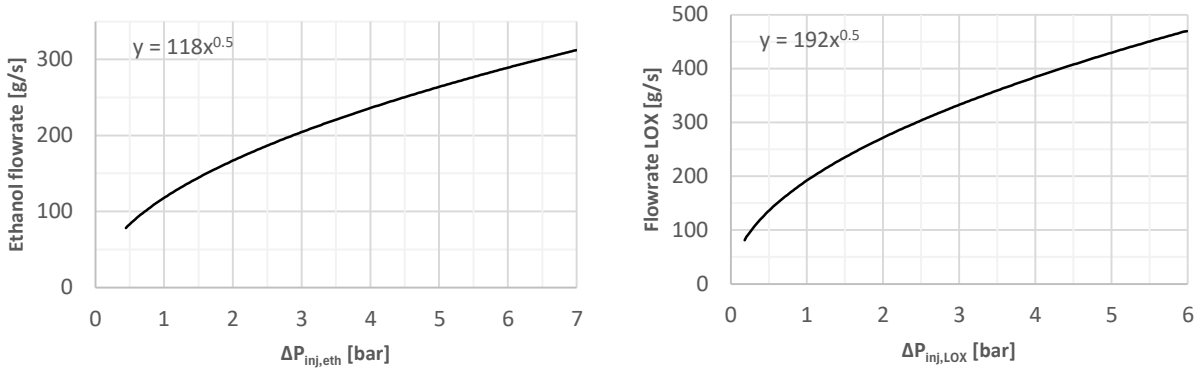

Figure 15: Mass flow rates as a function of injection pressure for Ethanol (left) and LOX (right)

Using the data in Table 1 and the K_{inj} for both injectors, we find that the injection pressure drop for the LOX should be $\Delta P_{LOX} = 2.43$ bar, and $\Delta P_{ETH} = 2.87$ bar for the ethanol.

Cryogenic flow tests with liquid nitrogen (LN2) were also used to determine the number of necessary chilldowns to have the cryogenic line cold enough for the LOX to stay liquid. A chilldown consists of opening the main LOX valve (SV13) for 1 second and waiting for 4 seconds. The 4s delay between each chilldown allows for the system to cool down as well as to accommodate the sensor response time, which avoids injecting more LOX or LN2 than necessary. This process is then repeated several times just before a hotfire test until the temperature of the outside of the pipe reaches a certain threshold, determined experimentally. Figure 16 shows a typical example of a chilldown right before a hotfire, where the threshold to continue the ignition sequence is set at -135°C.

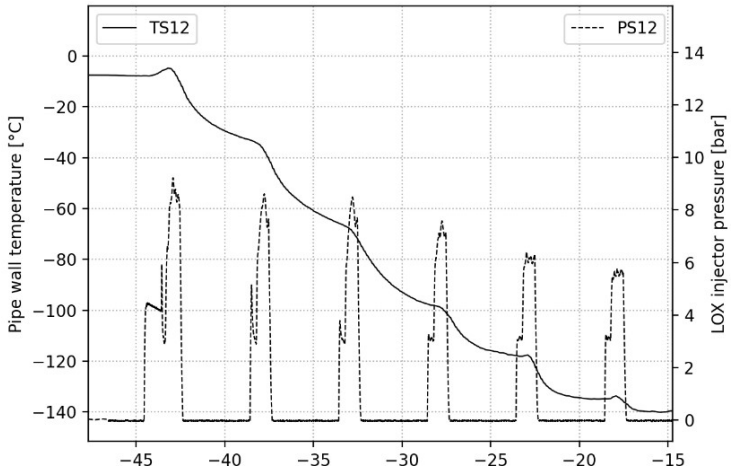

Figure 16**:** Chilldowns before test #2

4.3 Hotfire tests

The test campaign occurred over the course of three days between 08/05/2025 and 10/05/2025, with a total of 17 hotfire attempts summarized in Table 8. A total of four successful ignitions were achieved on the Battleship engine, with three full 5s burns. On the Arrax engine, two successful ignitions were achieved, with one full duration 5s hotfire. On the third day, longer burn durations of 10s and 30s were planned, but could unfortunately not be achieved due to ignition issues and lack of liquid nitrogen.

DOI: 10.13009/EUCASS2025-402

Table 8: Hotfire test campaign summary

#	Engine	Successful ignition	Burn duration	Notes
1	Battleship	No		Automatic abort due to target pressure not reached in time, ignition sequence adjusted.
2	Battleship	**Yes**	5 s	First successful hotfire, stable combustion reached after ~1s.
3	Battleship	**Yes**	5 s	Increased LOX tank pressure, stable combustion reached after ~1s.
4	Battleship	No		Igniter broke off before chamber ignition.
5	Battleship	No		Igniter failed to ignite.
6	Battleship	**Yes**	1 s	Ran out of ethanol after ~1s.
7	Battleship	**Yes**	5 s	Increased LOX tank pressure again, much faster ignition.
8	Arrax	No		Igniter failed to ignite.
9	Arrax	**Yes**	5 s	First successful ignition of Arrax, LOX tank pressure increased again, resulting in a much more transparent/purple flame.
10	Arrax	No		Igniter failed to ignite.
11	Arrax	No		Igniter broke off before chamber ignition.
12	Arrax	**Yes**	1 s	Very fast and smooth ignition, ran out of ethanol after ~1s.
13	Arrax	No		No ethanol due to a leak.
14	Arrax	No		Pressure spike at ignition caused igniter ejection prematurely.
15	Arrax	No		Pressure spike at ignition caused igniter ejection prematurely.
16	Arrax	No		Pressure spike at ignition caused igniter ejection prematurely.
17	Arrax	No		Pressure spike at ignition caused igniter ejection prematurely.

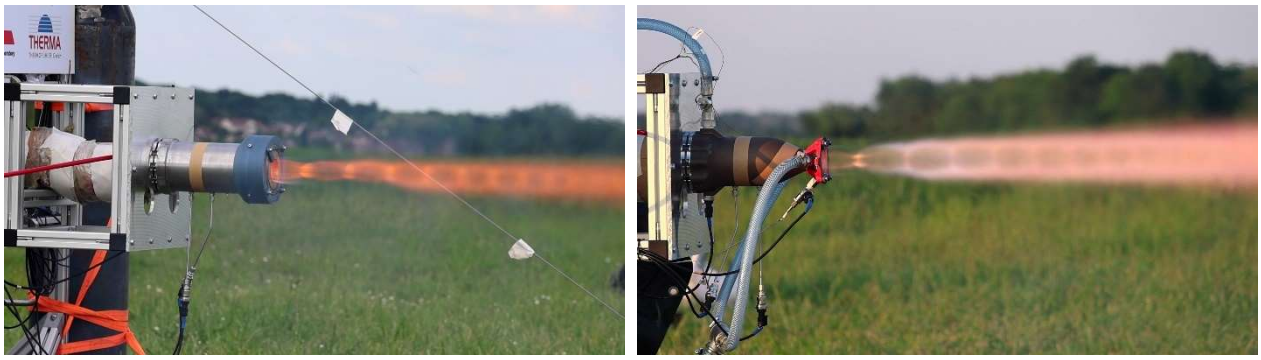

Figure 17: First hotfire of the Battleship (left), first hotfire of the Arrax (right), displaying the difference in flame color due to the higher O/F (1.5 vs 1.75)

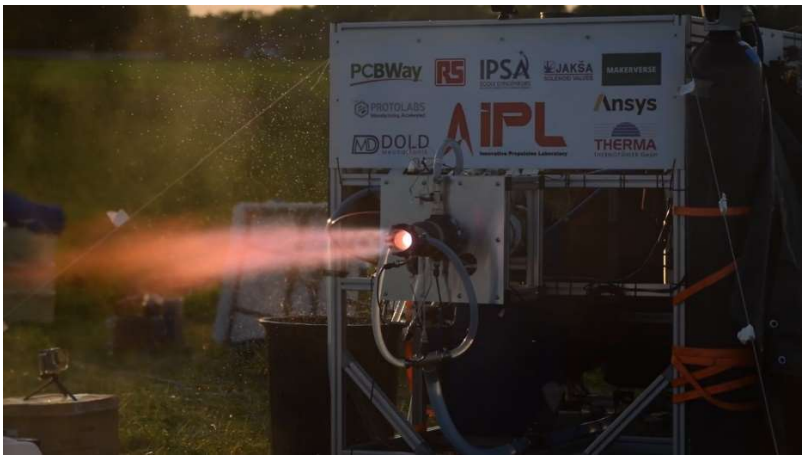

Figure 18: Second hotfire of the Arrax rocket engine

DOI: 10.13009/EUCASS2025-402

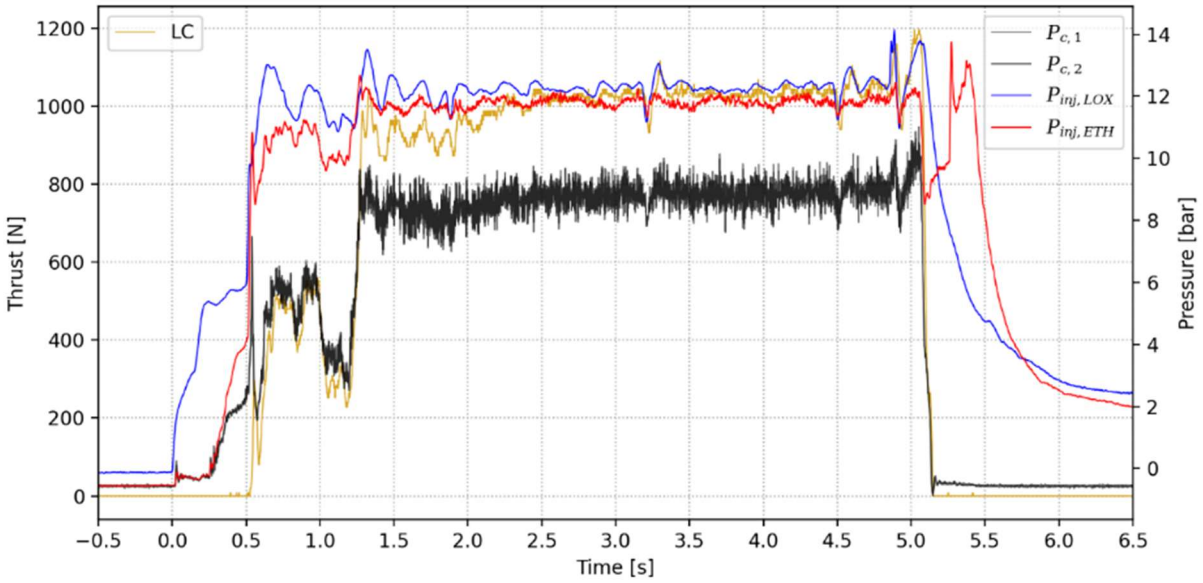

Figure 19: Measured Thrust, Injection and Chamber pressure for the test n°9

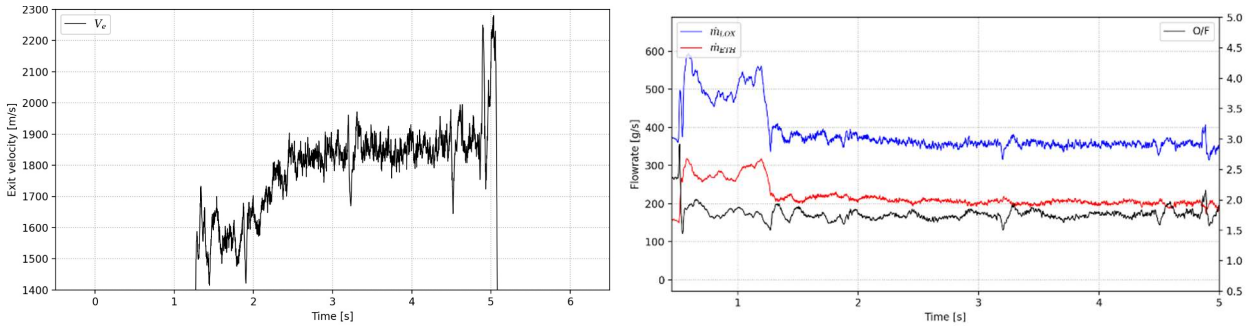

Figure 20: Calculated exhaust velocity (left and propellant mass flow rates and mixture ratio (right) for test n°9

For each test, the mass flow rate and O/F is deduced using the flow-pressure relationship established by cold flow tests and the injection pressure of each propellant. Unfortunately, the LOX injection pressure sensor malfunctioned during test #3, making computation of mass flow rate and mixture ratio impossible. Additionally, the third day (attempts #13 to #17), the ambient temperature was higher than the two previous days (25°C vs 13-15°C). Since the flash point of pure ethanol is around 13°C, we believe that the temperature increase caused the formation of flammable ethanol vapours inside the chamber prior to ignition. Furthermore, due to the injection of LOX during the chilldowns, it is believed a mixture of ethanol vapours and gaseous oxygen formed inside the chamber, which then ignited all at once when the igniter brought some energy, causing a pressure spike between 10 and 20 bar (depending on the test) inside the chamber, which broke the igniter off from the nozzle before propellant injection could even be initiated.

Using the temperature data from the outer surface of the engine during the hotfires of the Battleship, we can determine the temperature of the inner wall in the cylindrical part of the chamber as a function of time as well as the convection coefficient, assuming that no heat transfer to the ambient air occurs, by coding a simple 1D finite-difference solver and matching the temperature curves as shown in Figure 21. From this study, we find that the convection coefficient inside the cylindrical part of the chamber is about 380 $\mathrm{W/(m^2\ K)}$, which is about 40% of the value predicted by the Bartz equation.

From the cooling water temperature data in the Arrax hotfire, we can determine the total heat flux transferred to the water. We assume that no heat transfer occurs between the engine outer wall and the air and that steady state is reached by the end of the burn. The mass flow rate of water through the engine during test #9 was 1.5 kg/s. As can be seen in figure 22 below, the water is heated by $\Delta T_{water} = 21.5°\mathrm{C}$, resulting in a total heat flux of 134.9 kW.

DOI: 10.13009/EUCASS2025-402

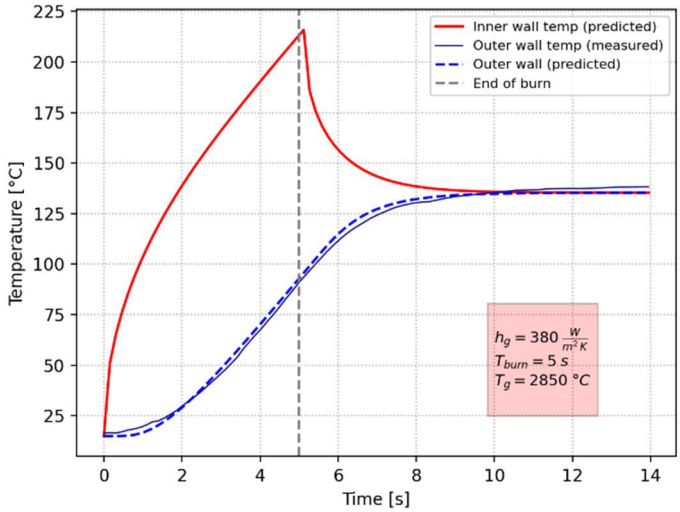

Figure 21: Inner wall temperature prediction and convection coefficient estimation for test #7

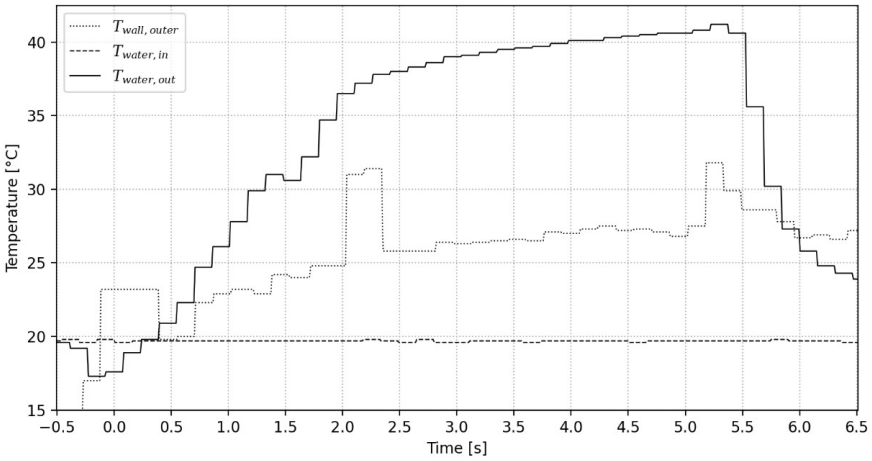

Figure 22: Cooling water temperature during test #9

In the CFD simulation, the average temperature of the water at the outlet is $T_{water,out} = 311.3$ K, and the average inlet temperature is $T_{water,in} = 293$ K. The mass flow rate in the simulation is $\dot{m}_{water} = 2$ kg/s, leading to a total heat flux of 153.1 kW. The relative difference between CFD and the experiment is therefore 11.8%, which again shows that the Bartz equation overpredicts the convective heat transfer coefficient in our case.

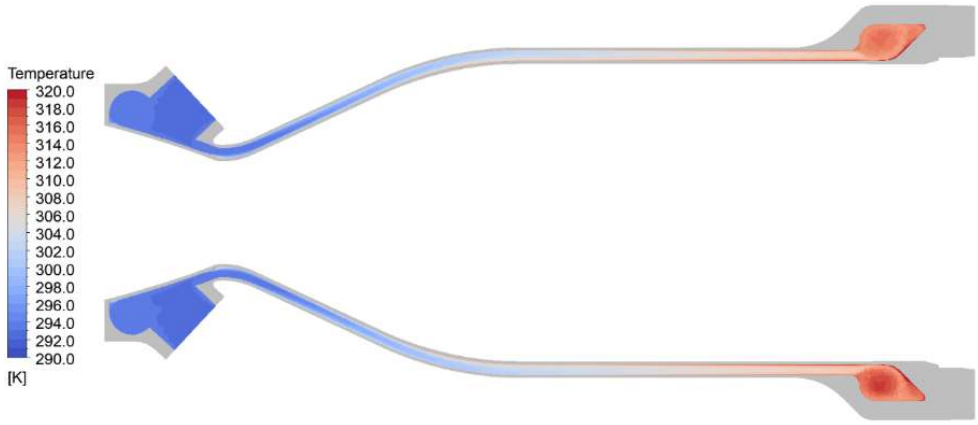

Figure 23: Water temperature variation inside the cooling channels at $\dot{m}_{water} = 2$kg/s.

DOI: 10.13009/EUCASS2025-402

5. Conclusion

This project successfully demonstrated the design, manufacture, and testing of a student-developed 1 kN-class regeneratively cooled LOX/ethanol rocket engine. The combination of analytical models, CFD simulations, and experimental data enabled us to reach ignition and steady-state operation, as well as assess heat transfer predictions, allowing us to develop future projects with more accuracy. Limitations included constraints on test duration due to logistical factors such as liquid nitrogen supply and ignition issues. This project provided the team with a functional test bench and its data acquisition system as well as precious hotfire data. Going forward, efforts will focus on increasing ignition reliability, extending burn duration, and improving combustion efficiency.

References

[1] P.Pempie. 2015. Moteurs-fusées à ergols liquides. *Centre National d'Études Spatiales*
[2] Sutton, G.P. and Biblarz, O. 2011. Rocket propulsion elements. *John Wiley & Sons*.
[3] A. Senott and C. Sharp. 2024. HCR5100 – Mojave Sphinx Build, Integration, and Launch Guidebook.
[4] Huzel, D.K. and Huang, D.H. 1992. Modern engineering for design of liquid-propellant rocket engines (Vol. 147). *AIAA*.
[5] Delpy, R. and Oswald, J., 2017. PERSEUS project 5 kN LOX/Ethanol rocket engine fire tests. In *7th European Conference for Aeronautics and Aerospace Sciences*.
[6] Radhakrishnan, K., Son, M., Lee, K. and Koo, J., 2018. Effect of injection conditions on mixing performance of pintle injector for liquid rocket engines. *Acta Astronautica*, *150*, pp.105-116.
[7] Chen, H., Li, Q. and Cheng, P., 2019. Experimental research on the spray characteristics of pintle injector. *Acta Astronautica*, *162*, pp.424-435.
[8] Erkal, B., Sumer, B. and Aksel, M.H., 2019. Design and Cold Flow Experiment Procedure of a Pintle Injector. *Proceedings of the AIAA Propulsion and Energy*, p.4117.
[9] Kenny, R., Moser, M., Hulka, J. and Jones, G., 2006, October. Cold flow testing for liquid propellant rocket injector scaling and throttling. In *42nd AIAA/ASME/SAE/ASEE Joint Propulsion Conference & Exhibit* (p. 4705).
[10] Andersson, E., 2022. Numerical Approach to the Design and Optimisation of a Bi-Propellant Pintle Injector.
[11] Mercieca, E., 2017. Spray Characteristics in Gas/Liquid Pintle Injection. *TU Delft, Delft*.
[12] Denies, L., 2015. Regenerative cooling analysis of oxygen/methane rocket engines
[13] Pizzarelli, M., 2008. Modeling of cooling channel flow in liquid-propellant rocket engines.
[14] Patel, N., Standbridge, S., Van Den Berghe, M. and Devalaraju, V., 2019. Design and additive manufacturing considerations for liquid rocket engine development. In *AIAA propulsion and energy 2019 forum* (p. 4392).
[15] Pizzarelli, M., 2017. Regenerative cooling of liquid rocket engine thrust chambers. *Agenzia Spaziale Italiana*.
[16] Kirchberger, C.U., 2014. Investigation on heat transfer in small hydrocarbon rocket combustion chambers
[17] Boysan, M.E., 2008. Analysis of regenerative cooling in liquid propellant rocket engines
[18] Juan, A.B. and Platero, A.L., 2023. Design of the regenerative cooling system for a 4kN LOX/Ethanol student-built liquid rocket engine.